

# Effect of an element addition on relaxation of elastic distortion based on particle-blocked grain boundary sliding

メタデータ	言語: eng 出版者: 公開日: 2017-10-03 キーワード (Ja): キーワード (En): 作成者: メールアドレス: 所属:
URL	<a href="http://hdl.handle.net/2297/9560">http://hdl.handle.net/2297/9560</a>

# Effects of Al<sub>3</sub>Sc particle size and precipitate-free zones on fatigue behavior and dislocation structure of an aged Al-Mg-Sc alloy

C. Watanabe<sup>1\*</sup>, R. Monzen<sup>1</sup> and K. Tazaki<sup>2</sup>

<sup>1</sup>Division of Innovative Technology and Science, Kanazawa University,  
Kakuma-machi, Kanazawa 920-1192, Japan

<sup>2</sup>Division of Environmental Science and Engineering, Kanazawa University,  
Kakuma-machi, Kanazawa 920-1192, Japan

\* Corresponding author, e-mail: [chihiro@t.kanazawa-u.ac.jp](mailto:chihiro@t.kanazawa-u.ac.jp)

Fax: +81-76-264-6495

Tel: +81-76-234-4680

## Abstract

Al-Mg-Sc alloy polycrystals have been cyclically deformed at room temperature under constant stress amplitudes. Cyclic softening after initial hardening is found in specimens with small particles of 4 nm, but no cyclic softening takes place in specimens with large particles of 11 nm. Transmission electron microscopy observations reveal that dislocations are uniformly distributed under all applied stress amplitudes in the specimens containing large particles, whereas clearly developed slip bands are formed in the cyclically softened specimens bearing small particles. Two-step aging causes a decrease in the width of precipitate-free zones in the large-particle specimen, resulting in the improvement of fatigue life.

*Keywords:* Al-Mg-Sc alloy, Dislocation structure, Cyclic softening, Stress amplitude

## 1. Introduction

The addition of a small amount of Scandium (Sc) to Al-Mg alloys causes a significant increase in the strength of the alloys, due to the existence of coherent, finely dispersed  $L1_2$   $Al_3Sc$  precipitates [1-3]. Although several experiments have been performed on the mechanical properties of Al-Mg-Sc ternary alloys, there are few investigations of the fatigue properties of these alloys.

In a previous paper [4], we examined the low-cycle fatigue behavior and dislocation microstructure under plastic-strain-controlled fatigue conditions, using an aged Al-Mg-Sc alloy with finely dispersed, spherical  $Al_3Sc$  particles of different diameters, i.e. 4 and 11 nm. The alloy with 11 nm particles showed cyclic hardening to saturation despite the fact that the  $Al_3Sc$  particles were coherent. On the other hand, cyclic softening occurred in the alloy with 4 nm particles under large plastic strain amplitudes of above  $1 \times 10^{-4}$ . To establish a multifunctional method for fatigue life assessments, it is very useful to know the similarities and differences between stress- and strain-controlled fatigue behaviors.

In this study, a polycrystalline Al-Mg-Sc alloy with dispersed  $Al_3Sc$  particles is cyclically deformed at room temperature under various constant stress amplitudes, and the dislocation structure is investigated in relation to the stress-strain responses. As in the previous study, the two particle diameters of 4 and 11 nm have been selected. In addition, the effect of two-step aging on fatigue life is examined.

## 2. Experimental procedures

Specimens for fatigue tests were cut from hot-rolled polycrystalline Al-1mass%Mg-0.27mass%Sc alloy plates with the stress axis parallel to the rolling direction. These specimens were solutionized at 905 K for  $7.2 \times 10^3$  s and water quenched. Transmission electron microscopy (TEM) observations revealed that no precipitates existed in the solution treated specimens. To obtain spherical and coherent  $Al_3Sc$  particles, one set of

solutionized specimens was aged at 573 K for  $9.0 \times 10^2$  s, and second set was aged at 623 K for  $6.48 \times 10^4$  s, corresponding to under-aging and over-aging conditions which produced almost the same Vickers hardness of 70. Hereafter, these under-aged and over-aged specimens will be referred to as specimens UA and OA, respectively. The average diameter of  $\text{Al}_3\text{Sc}$  particles in specimens UA was 4 nm, while the particle diameter in specimen OA averaged 11 nm. The average size was determined from TEM observations of over 200 particles. In addition another set of solution-treated specimens underwent a two-step aging treatment, that is, aging at 573 K for  $3.0 \times 10^2$ , water quenching, and then aging at 623 K for  $6.48 \times 10^4$  s. This two-step aging produced  $\text{Al}_3\text{Sc}$  particles with the same diameter of 11 nm. The two-step-aged specimen will be referred to as specimen OA2. Judging from the Al-Sc equilibrium phase diagram [5], the volume fractions of the  $\text{Al}_3\text{Sc}$  particles in specimens UA, OA and OA2 are nearly identical and are estimated as 0.007.

All mechanical tests were carried out at room temperature in air. Tensile properties were determined with an initial strain rate of  $3.0 \times 10^{-3} \text{ s}^{-1}$ . Fully-reversed tension-compression fatigue tests were performed under stress-amplitude control. The ramp loading method [6] was adopted and the ramp loading length was set to 30 cycles. A low frequency of 0.5 Hz was employed when the tests were started and the frequency was increased up to 10 Hz after several tens of cycles. The stress-strain hysteresis loops were monitored with a digital oscilloscope.

The fatigued specimens were sliced into 3mm disks parallel to the stress axis and were mechanically ground down to 0.2 mm. Thin foils for TEM observations were prepared by electro-polishing. Microscopy was performed with JOEL-2000EX and JOEL-2010FEF microscopes operating at 200 kV.

### **3. Results**

#### *3.1. Mechanical properties*

The solutionized and aged specimens were coarse-grained with an equiaxed grain size of 0.5 to 1 mm. The Al-Mg-Sc ternary equilibrium phase diagram [7] shows that Mg in the present Al-1mass%Mg-0.27mass%Sc alloy does not form any compounds at the aging temperatures examined. In fact, aging of the alloy at 573 and 623 K produced only spherical Al<sub>3</sub>Sc particles in the Al matrix. As seen in the high-resolution TEM images in Figs. 1 (a) and (b), the Al<sub>3</sub>Sc particles of 4 or 11 nm in diameter were completely coherent with the Al matrix. These observations are consistent with those in the literature [8].

Fig. 2 presents the stress-strain curves of specimens UA and OA. For comparison, the result for a Sc-free Al-1mass%Mg alloy is also shown [9]. The contribution of the Al<sub>3</sub>Sc particles to the strength of the Al-Mg alloy is apparent. The value of 0.2% proof stress for specimen UA is slightly larger than that for specimen OA. However, the work-hardening rate of specimen OA is larger than that of specimen UA and, as a result, the tensile stresses of the specimens are reversed. The difference in the work-hardening rate between the specimens UA and OA reflects the different strengthening mechanisms, which depend on the particle size. Marquis *et al.* examined yield strength at room temperature in an Al-2mass%Mg-0.2mass%Sc alloy containing coherent Al<sub>3</sub>Sc particles with a mean diameter between 4 and 25 nm [10]. The dependence of the yield stress on particle size was explained using classical precipitation-strengthening theory. The theory predicts a transition from particle shearing to Orowan dislocation looping mechanisms at a particle diameter of 4.8 nm at room temperature, in good agreement with experimental data. This indicates that glide dislocations may cut through Al<sub>3</sub>Sc particles in the specimen UA, but move around the particles so as to by-pass them in the specimen OA.

Fatigue tests under stress-amplitude control were performed at various constant stress amplitudes. The cyclic-deformation curves of specimens OA and UA are shown in Figs. 3 (a) and (b), where the plastic strain amplitude  $\epsilon_{a,pl}$  is plotted against the number of fatigue cycles ( $N$ ). In the case of stress-controlled tests, the decrease of  $\epsilon_{a,pl}$  against  $N$  means cyclic

hardening, and the increase of  $\varepsilon_{a,pl}$  corresponds to cyclic softening. For comparison, the cyclic-deformation curve of a binary Al-1mass%Mg alloy fatigued under a stress amplitude ( $\sigma_a$ ) of 55 MPa is also indicated in Fig. 3 (a). The value of  $\sigma_a / \sigma_{0.2}$  for the Al-Mg alloy is about 0.6, which is nearly identical to that of  $\sigma_a / \sigma_{0.2}$ , where  $\sigma_a = 90$  MPa for the specimens UA and OA.

In the Al-Mg alloy, monotonic hardening can be seen. The hardening rate for the Al-Mg alloy is initially low and then rapidly increases after a certain number of cycles. This behavior is consistent with the result of a single phase Al alloy fatigued under stress-controlled fatigue tests [11]. On the other hand, in the specimens OA, the  $\varepsilon_{a,pl}$  decreases rapidly with increasing  $N$  and finally reaches saturation at all applied stress amplitudes. In contrast, the cyclic deformation curves of specimens UA show initial hardening and then clear cyclic softening at all stress amplitudes. To examine whether such softening in the specimens UA is an effect of or associated with cracking, a test was conducted on a specimen UA at  $\sigma_a = 90$  MPa; the fatigue test was suspended after commencement of softening. The specimen surface was electro-polished, and then the specimen underwent further cycling. This process was repeated twice, as shown in Fig. 4. Each time the cycling was stopped, the surface showed slip bands like those shown in Fig. 5 (b). After polishing, the surface was again smooth and entirely free of defects.

It should be noted from Fig. 4 that the values of  $\varepsilon_{a,pl}$  on stopping during softening are comparable with those of the subsequent cycles after re-polishing. As further cycles are applied, the values of  $\varepsilon_{a,pl}$  gradually increase. Therefore, it is apparent that the softening is not caused by surface crack initiation but is the essential character of the specimen UA. If the softening were due to the presence of cracks,  $\varepsilon_{a,pl}$  should have immediately attained the minimum on restarting cycling after each polishing treatment.

The hardening-saturation and hardening-softening sequences of specimens OA and UA under stress-controlled tests are similar to those of the strain-controlled tests previously

conducted [4]. Clearly, these results are caused by the difference in the size of the  $\text{Al}_3\text{Sc}$  particles, and are related to the interaction mode with glide dislocations. In the previous strain-controlled test with a small  $\varepsilon_{a,pl}$  of  $1 \times 10^{-4}$ , however, both the specimens OA and UA exhibited cyclic hardening to saturation where the stress level reached about 90 MPa [4]. In the present study, in contrast, the specimen UA shows cyclic softening even at the smallest  $\sigma_a$  of 70 MPa.

### 3.2 Microstructures

The difference in the particle size affects not only the mechanical behavior but also the surface slip features. The surface appearances of specimens UA and OA fatigued at  $\sigma_a = 90$  MPa are presented in Figs. 5 and 6. Fig. 5 (a) shows the surface slip feature of a specimen UA fatigued up to  $N = 5000$  (half-way down to the minimum  $\varepsilon_{a,pl}$ ). Slip bands are formed in a portion of grains. When the number of cycles is increased up to  $N = 10000$  (at minimum  $\varepsilon_{a,pl}$ ), almost all grains have slip bands (Fig. 5 (b)). Some of them are deeply marked, but actual cracking was not observed. At fracture, the sharp slip bands are seen in all grains (Fig. 5 (c)).

These results are due to the slip bands being formed even at the initial stage of hardening in the grains which have nearly maximum shear orientations. As further cycling is applied, these grains work-harden. As a result, most of the imposed deformation is accommodated by the grains with orientations which deviate from the direction of maximum shear. This process continues until most grains are hardened and marked with slip bands. Finally, the minimum  $\varepsilon_{a,pl}$  is attained.

On the other hand, all of the specimens OA with cyclic-hardening to saturation display no slip bands, as shown in Fig. 6. The macroscopic cracks nucleated and propagated predominantly along the grain boundaries in the specimen OA, but the crack nucleation in the specimen UA occurred almost exclusively along the slip bands.

Fig. 7(a) depicts dislocation microstructures for the specimen UA cyclically

deformed under a constant stress amplitude of  $\sigma_a = 90$  MPa. At the early stage of fatigue just after ramp loading, loose slip bands parallel to the trace of the primary slip plane have already formed in a portion of grains, as shown in Fig. 7(a). More than 20 grains were observed to determine their orientations with respect to the stress axis. Similar to the surface observations, such slip bands were observed only in the grains with single slip orientations. In all of the grains examined, distinct dislocation structures such as veins, labyrinths, ladders or cells were not clearly developed. This shows the effectiveness of  $\text{Al}_3\text{Sc}$  particles in preventing the formation of a geometrically regular dislocation arrangement.

As the fatigue deformation proceeds and the cyclic softening starts, well-developed slip band structures form within almost all grains, as shown in Fig. 7(b). This corresponds to the observation of slip bands on the surface of cyclically softened specimen UA in Fig. 5(c). So-called cell structure is seen within the slip bands in Fig. 7(b). Since the black and white contrasts change from cell to cell, misorientations are generated. The specimens fatigued under  $\sigma_a = 70$  and 120 MPa exhibited a similar evolution of the dislocation structure. In the plastic-strain-controlled fatigue tests of the Sc-free Al-Mg alloy, such cell structures were observed only at plastic strain amplitudes larger than  $5.0 \times 10^{-3}$  [9]. As can be seen in Fig. 3, the average  $\varepsilon_{\text{apl}}$  of the whole gauge section of specimen UA fatigued at 90 MPa just before fracture is about  $1.0 \times 10^{-4}$ . This fact indicates that strong strain localization occurs within the slip band.

Fig. 8 shows a TEM image of specimen OA fatigued to failure at  $\sigma_a = 120$  MPa. Unlike specimen UA, no slip bands are visible. Dislocations are uniformly distributed and only tangled dislocations formed around the particles (see the inset of Fig. 8), even when the largest  $\sigma_a$  of 120 MPa was employed. Furthermore, dislocation microstructures under three different stress amplitudes exhibited no significant differences. As the  $\sigma_a$  increased, the only detectable change in dislocation microstructures was the increase in the density of dislocations tangled around the particles. There are no indications of inhomogeneous

deformation. The uniform dislocation structures in specimen OA reflect the difficulty in dislocations rearranging due to the relatively large Al<sub>3</sub>Sc particles.

As mentioned in Section 3.1, the small Al<sub>3</sub>Sc particles in specimen UA can be cut by dislocations. As a result, partially reversible to-and-fro motion of glide dislocations results in the destruction and re-dissolution of the particles, and thus the local resistance against the dislocation motion decreases. Local softening usually leads to strain localization and inhomogeneous deformation [12, 13]. To check whether such particle shearing occurred in the specimen UA during fatigue tests, the average size of the Al<sub>3</sub>Sc particles within the slip bands or in the matrix was measured by TEM using the specimen UA re-aged at 573 K for  $9 \times 10^2$  s following a fatigue test to failure at  $\sigma_a = 90$  MPa. The resulting average particle diameters were 4 nm within the slip bands and 7 nm in the matrix. This discrepancy in the particle size implies that the small Al<sub>3</sub>Sc particles in specimen UA were chopped by dislocations within the strongly strained slip bands and were precipitated by the short re-aging treatment. The cyclic softening in specimen UA in Fig. 3 can then be explained by a loss of particle strengthening through particle re-dissolution in the slip bands.

On the other hand, when the particles become larger, dislocations must by-pass the particles by the Orowan mechanism. We can see from Fig. 3 that at the early stage of fatigue, the decrease in  $\epsilon_{ap1}$  in the specimens OA is steeper than in the specimens UA. This is explained by a rapid formation of Orowan loops around the relatively large particles. In this case, the particles act as strong obstacles against the dislocation motion and rearrangement (Fig. 8), and deformation becomes very homogeneous (Fig. 6), in agreement with the prediction from the elastic energy method for unidirectionally deformed metals containing non-sharable particles by Mori and Mura [14]. This may result in the absence of the cyclic softening.

### *3.3. Effect of two-step aging on fatigue life*

The results of fatigue life tests ( $S$ - $N$  curves) for specimens UA and OA are shown in Fig. 9, where the cyclic stress amplitude  $\sigma_a$  is plotted as a function of the number of cycles to failure ( $N_f$ ). Since slip bands are known as sites for crack initiation, as would be expected, the specimen OA shows more enhanced fatigue life than the specimen UA, owing to the more homogeneous deformation behavior of the specimen OA compared with the specimen UA.

In the specimen OA, precipitate-free zones (PFZs) were formed near the grain boundaries [4]. In the addition to the difference in  $\text{Al}_3\text{Sc}$  particle sizes as mentioned above, the existence of PFZs can be pointed out as another factor affecting fatigue life. Since the PFZs have much less strength than the grain interior, dislocation movement seems to occur preferentially within the PFZs. As we can see in Fig. 10, the dislocation density within the PFZ is higher than that of the grain interior in the specimen OA. From analyses of Kikuchi lines and diffraction patterns, it was found that misorientations of a few degrees developed between the PFZs and the matrix around the PFZs. This indicates that strain localization took place within the PFZ. It is likely that the existence of PFZs has a detrimental influence on the fatigue life of specimen OA.

Table 1 lists the average diameter of  $\text{Al}_3\text{Sc}$  particles, the average width of PFZs and the tensile properties for the specimen OA, aged at 623 K for  $6.48 \times 10^4$  s, and the specimen OA2, two-step aged at 573 K for  $3.0 \times 10^2$  and then at 623 K for  $6.48 \times 10^4$  s. The two-step aging does not essentially change the strength but does increase the elongation. Also, the width of PFZs is reduced by the two-step aging. Comparison between the  $S$ - $N$  curves of specimens OA and OA2 in Fig. 9 shows that the two-step aging results in enhanced fatigue life. Therefore we conclude that the decrease in the PFZ width brings about the increase in the fatigue life.

## 5. Conclusions

Fatigue tests of an aged Al-Mg-Sc alloy containing  $\text{Al}_3\text{Sc}$  particles with average

diameters 4 and 11 nm were carried out under constant stress amplitudes. The results and conclusions are summarized as follows.

- (1) Cyclic softening appears in specimens with  $\text{Al}_3\text{Sc}$  particles of 4 nm at any applied stress amplitudes, whereas specimens with  $\text{Al}_3\text{Sc}$  particles of 11 nm show cyclic hardening to saturation.
- (2) Dislocations are very uniformly distributed in large-particle specimens, while slip bands are observed in small-particle specimens.
- (3) The fatigue softening of small-particle specimens is unambiguously related to the partial re-dissolution of the  $\text{Al}_3\text{Sc}$  particles within the slip bands and not due to surface cracking.
- (4) Two-step aging decreases the width of precipitate-free zones in the specimen with large particles, and as a result the fatigue life is enhanced.

## **Acknowledgements**

The results presented in this work are part of a research project financially supported by the Mazda foundation. This work was supported in part by a Grant-in-Aid for Young Scientist (B) from Japan Society for Promotion of Science (JSPS). The authors wish to acknowledge Kobe Steel Ltd. for supplying the specimens.

## References

- [1] Sawtell RR, Jensen CL. Mechanical properties and microstructures of Al-Mg-Sc alloys. *Metal Trans A* 1990;21(2):421-430.
- [2] Elagin VI, Zakharov VV, Rostova TD. Scandium-alloyed aluminum alloys. *Met Sci Heat Treat* 1992;34(1):37-45.
- [3] Lathabai S, Lloyd PG. The effect of scandium on the microstructure, mechanical properties and weldability of a cast Al-Mg alloy. *Acta Mater* 2002;50(17):4275-4292.
- [4] Watanabe C, Jin CY, Monzen R, Kitagawa K. Low-cycle fatigue behavior and dislocation structure of an Al-Mg-Sc alloy. *Mater Sci Eng A* 2004;387-389:552-555.
- [5] Murray JL. The Al-Sc (aluminum-scandium) system. *J Phase Equilib* 1998;19(4):380-384.
- [6] Llanes L, Laird C. Substructure evolution of copper polycrystals under different testing conditions: conventional strain control and ramp loading. *Mater Sci Eng A* 1993;161(1):1-12.
- [7] Handbook of ternary alloy phase diagrams. Villars P, Prince A, Okamoto H, editors. Materials Park, OH:ASM, 1995, pp. 3900-3902.
- [8] Watanabe C, Watanabe D, Monzen R. Coarsening behavior of Al<sub>3</sub>Sc precipitates in an Al-Mg-Sc alloy. *Mater Trans* 2006;47(9):2285-2291.
- [9] Jin CY. The effect of Sc addition on low-cycle fatigue behavior and dislocation structure of an Al-Mg alloy. Master's Theses, Kanazawa University, 2003. p. 22.
- [10] Marquis EA, Seidman DN, Dunand DC. Effect of Mg addition on the creep and yield behavior of an Al-Sc alloy. *Acta Mater* 2003;51(16): 4751-4760.
- [11] Fujii T, Watanabe C, Nomura Y, Tanaka N, Kato M, *Mater Sci Eng A* 2001;319-321:592-596.
- [12] Calabrese C, Laird C. Cyclic stress-strain response of two-phase alloys: Part I. Microstructures containing particles penetrable by dislocations. *Mater Sci Eng* 1974;13(2): 141-157.
- [13] Steiner D, Gerold V. The fatigue behavior of age-hardened Cu-2at.%Co alloy. *Mater Sci*

Eng 1986;84: 77-88.

[14] Mori T, Mura T. Slip morphology in dispersion hardened materials. Mater Sci Eng  
1976;26(1):89-93.

## Figure and table captions

Fig. 1 High-resolution TEM images of Al<sub>3</sub>Sc particles in specimens (a) UA and (b) OA. Both images were taken along the [100]<sub>Al</sub> zone axis.

Fig. 2 Stress-strain curves of specimens UA and OA. For comparison, the curve of a Sc-free Al-1mass%Mg alloy is also presented.

Fig. 3 Cyclic-deformation curves of specimens (a) OA and (b) UA obtained under various stress amplitudes. The curve of a Sc-free Al-1mass%Mg alloy fatigued at 55 MPa is also shown in (a).

Fig. 4 Cyclic-deformation curve of specimens UA fatigued at  $\sigma_a = 90$  MPa. The open squares indicate interruptions for surface re-polishing.

Fig. 5 Surface slip morphologies of specimen UA fatigued at  $\sigma_a = 90$  MPa until (a)  $N = 5000$ , (b)  $N = 10000$  and (c) failure. All images were taken from the same area.

Fig. 6 Surface slip morphology of specimen OA fatigued at  $\sigma_a = 90$  MPa to failure.

Fig. 7 TEM images taken from specimens UA fatigued at  $\sigma_a = 90$  MPa (a) until  $N = 35$  and (b) to failure. The stress axis is indicated by the arrow in (b).

Fig. 8 TEM image taken from specimen OA fatigued at  $\sigma_a = 120$  MPa to failure. The inset shows a magnified weak beam image. The stress axis is indicated by the arrow.

Fig. 9 *S-N* curves of specimens UA, OA and OA2.

Fig. 10 TEM image of a PFZ along a grain boundary in specimen OA fatigued at  $\sigma_a = 120\text{MPa}$  to failure.

Table 1 Values of the average diameter of  $\text{Al}_3\text{Sc}$  particles and width of PFZs, and mechanical properties for specimens OA and OA2.

Table 1

	Specimen OA	Specimen OA2
Particle diameter	11 nm	11 nm
PFZ width	200 nm	110 nm
<hr style="border-top: 1px dashed black;"/>		
$\sigma_{0.2}$	142 MPa	143 MPa
$\sigma_{\text{UTS}}$	209 MPa	211 MPa
$\varepsilon_f$	0.26	0.31

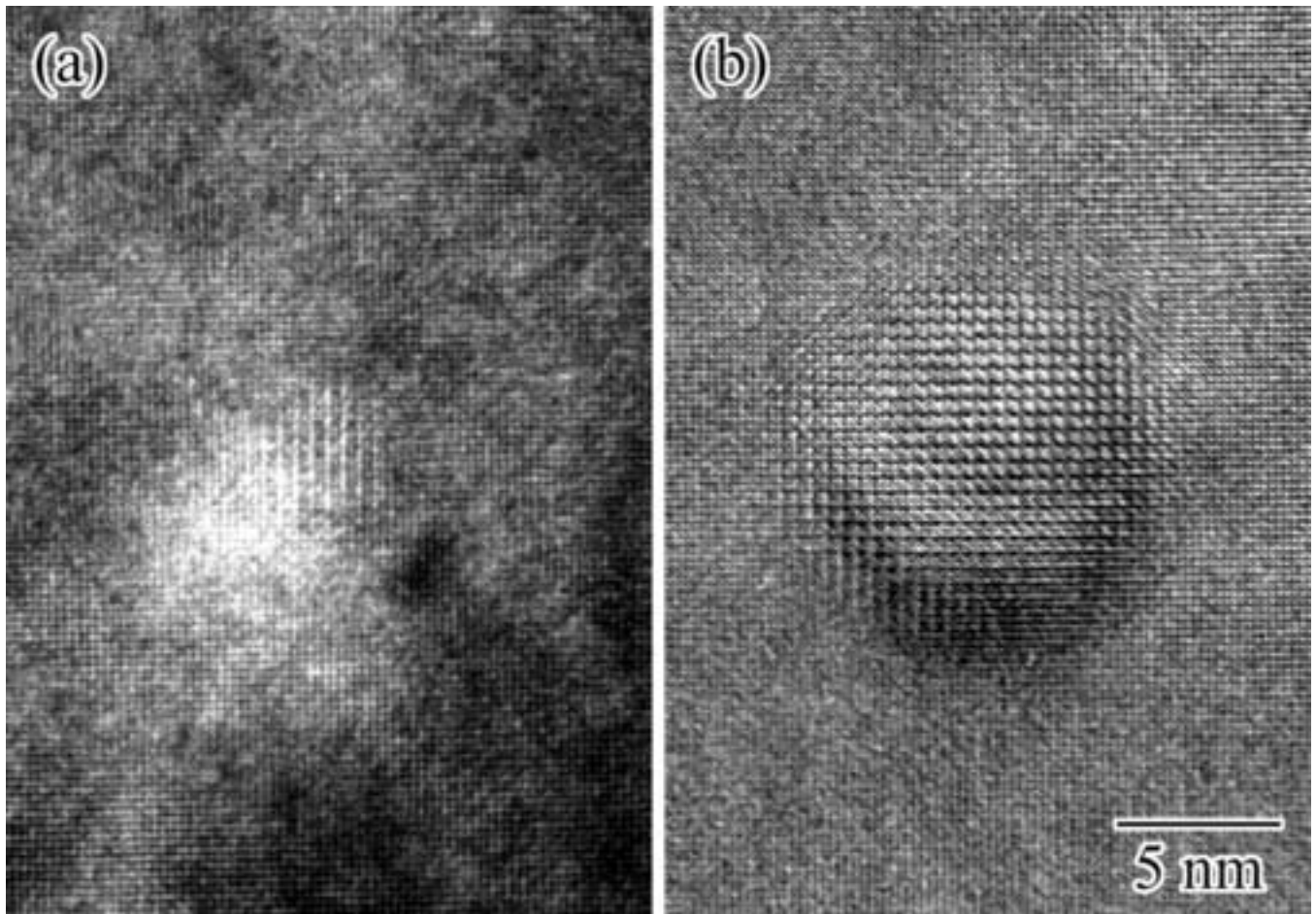


Figure02

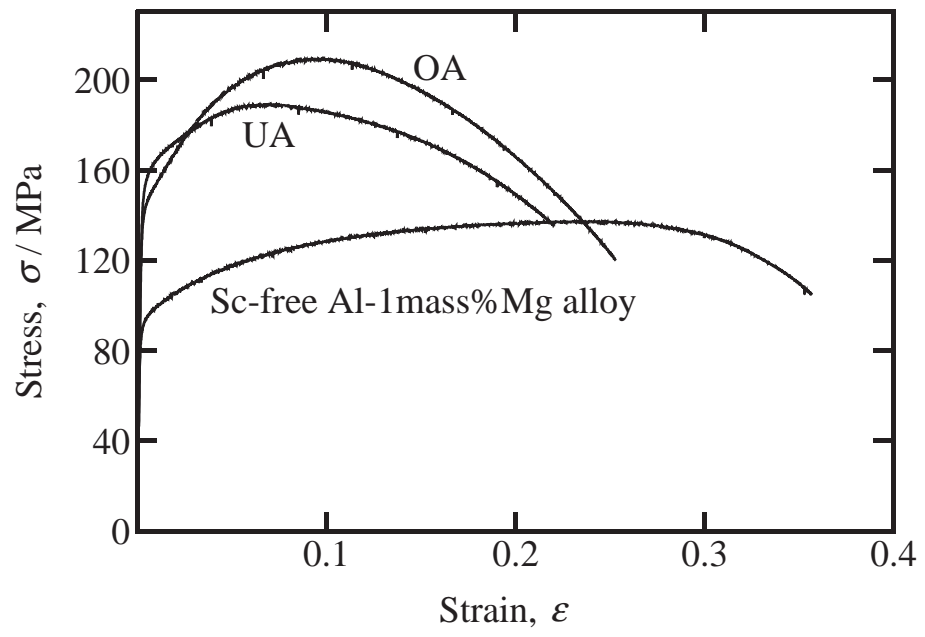
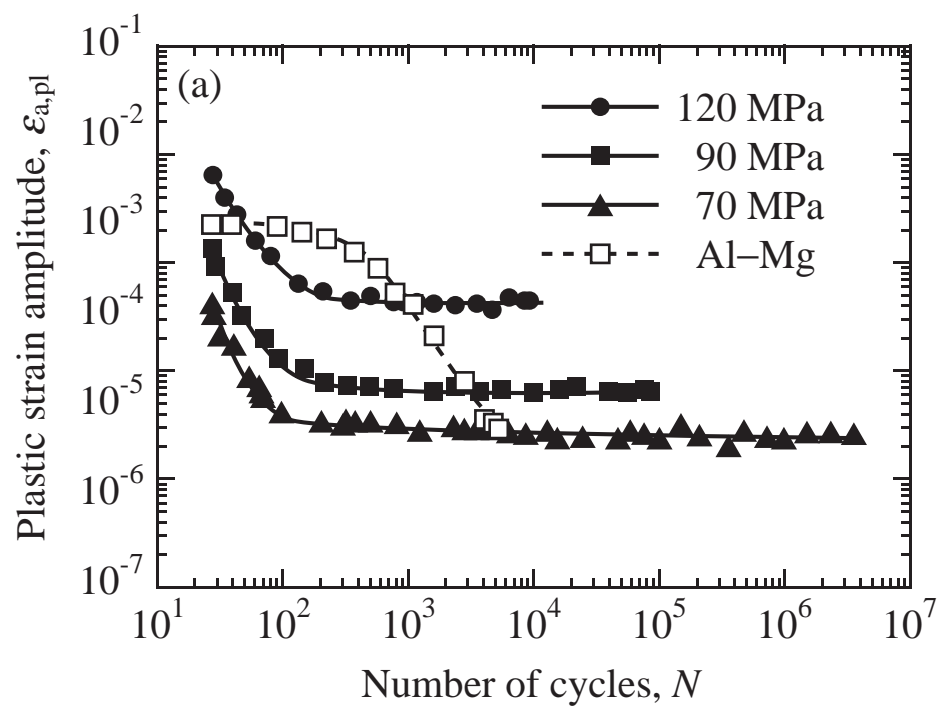


Figure03\_a



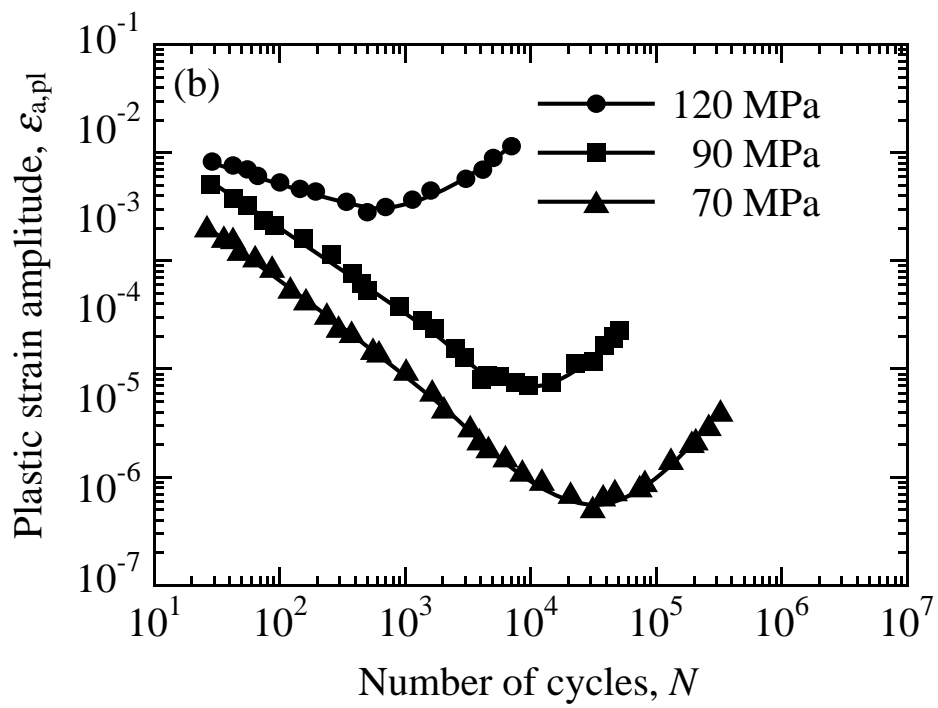
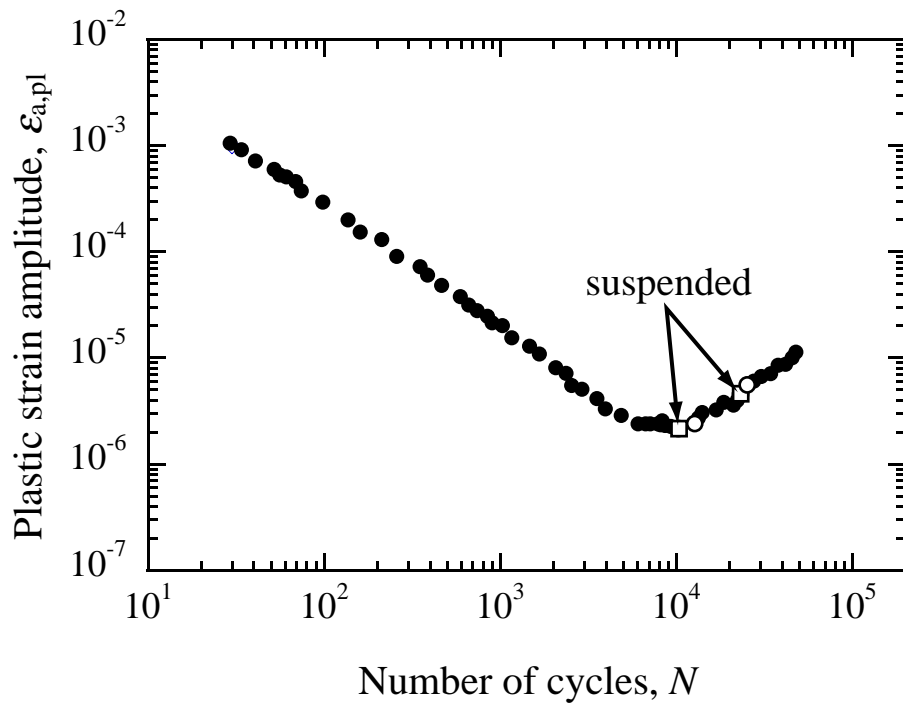
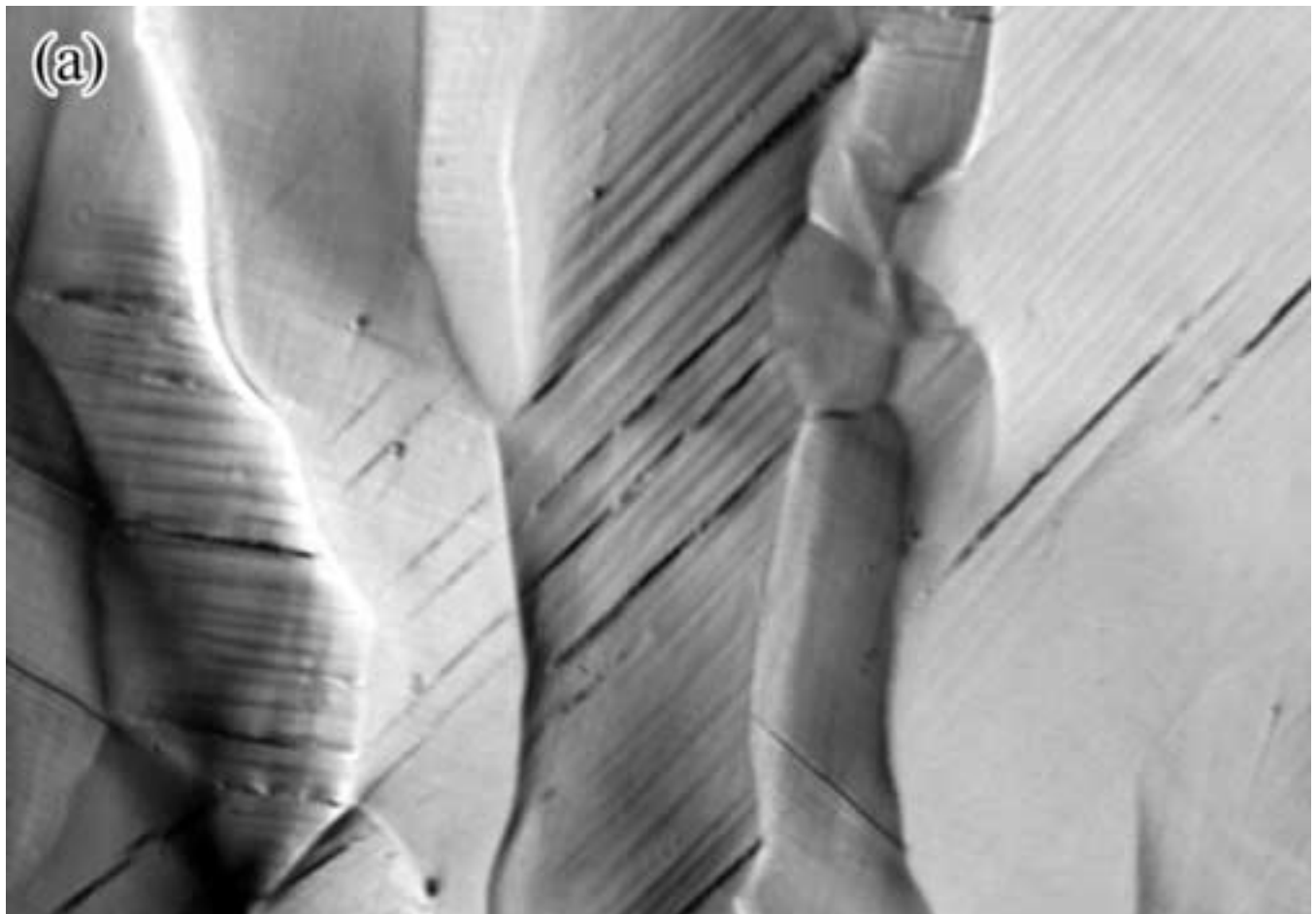
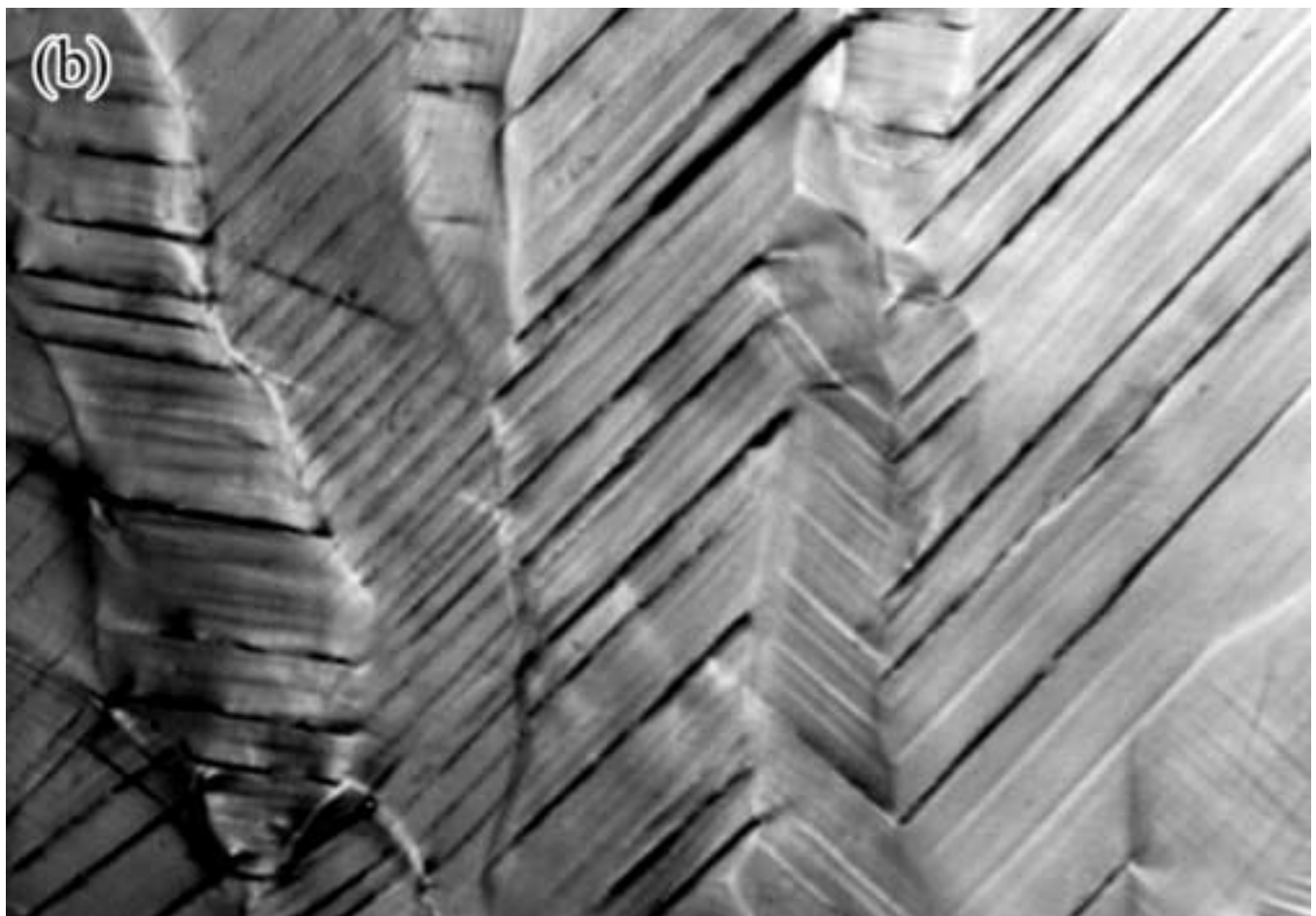


Figure04







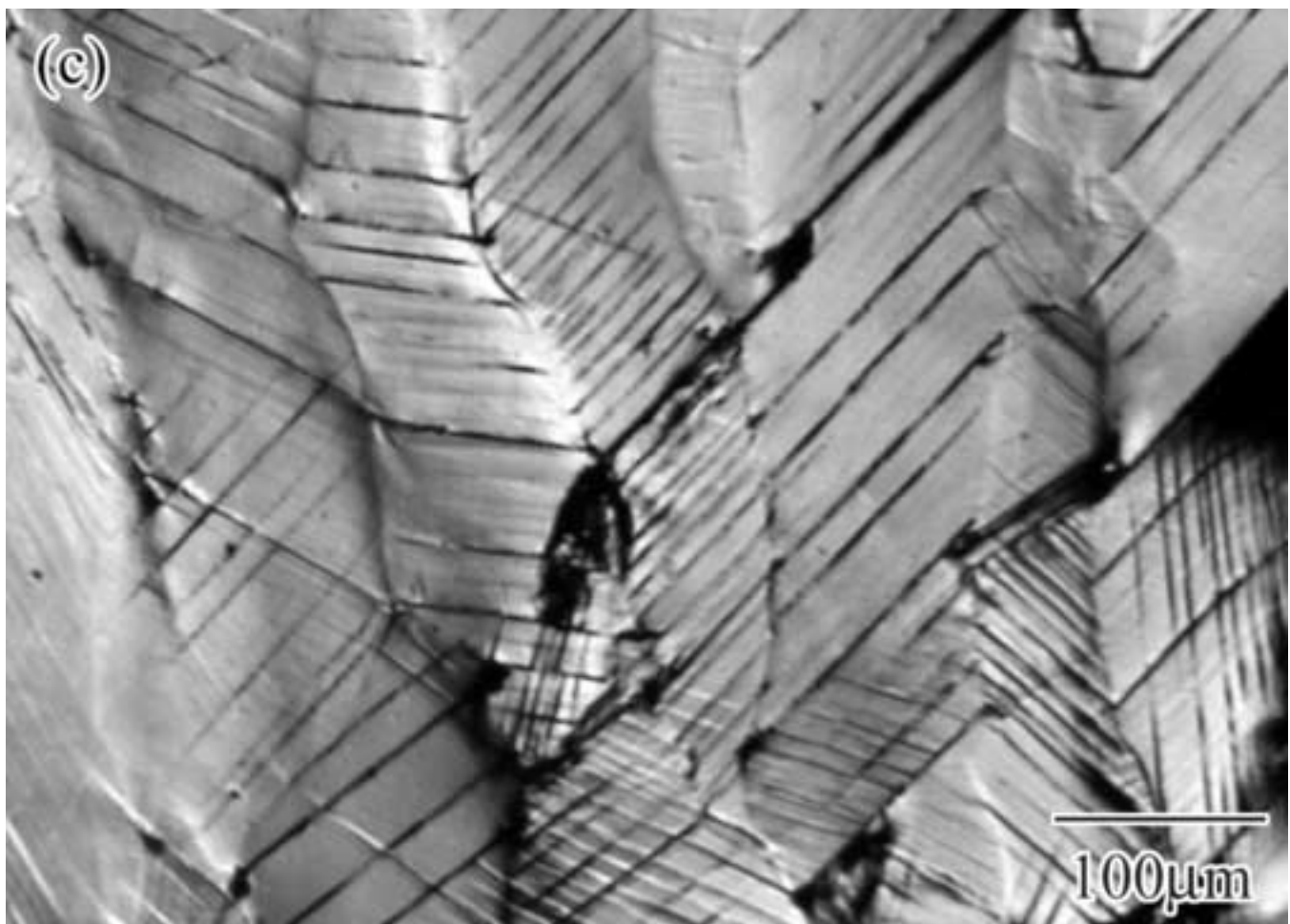
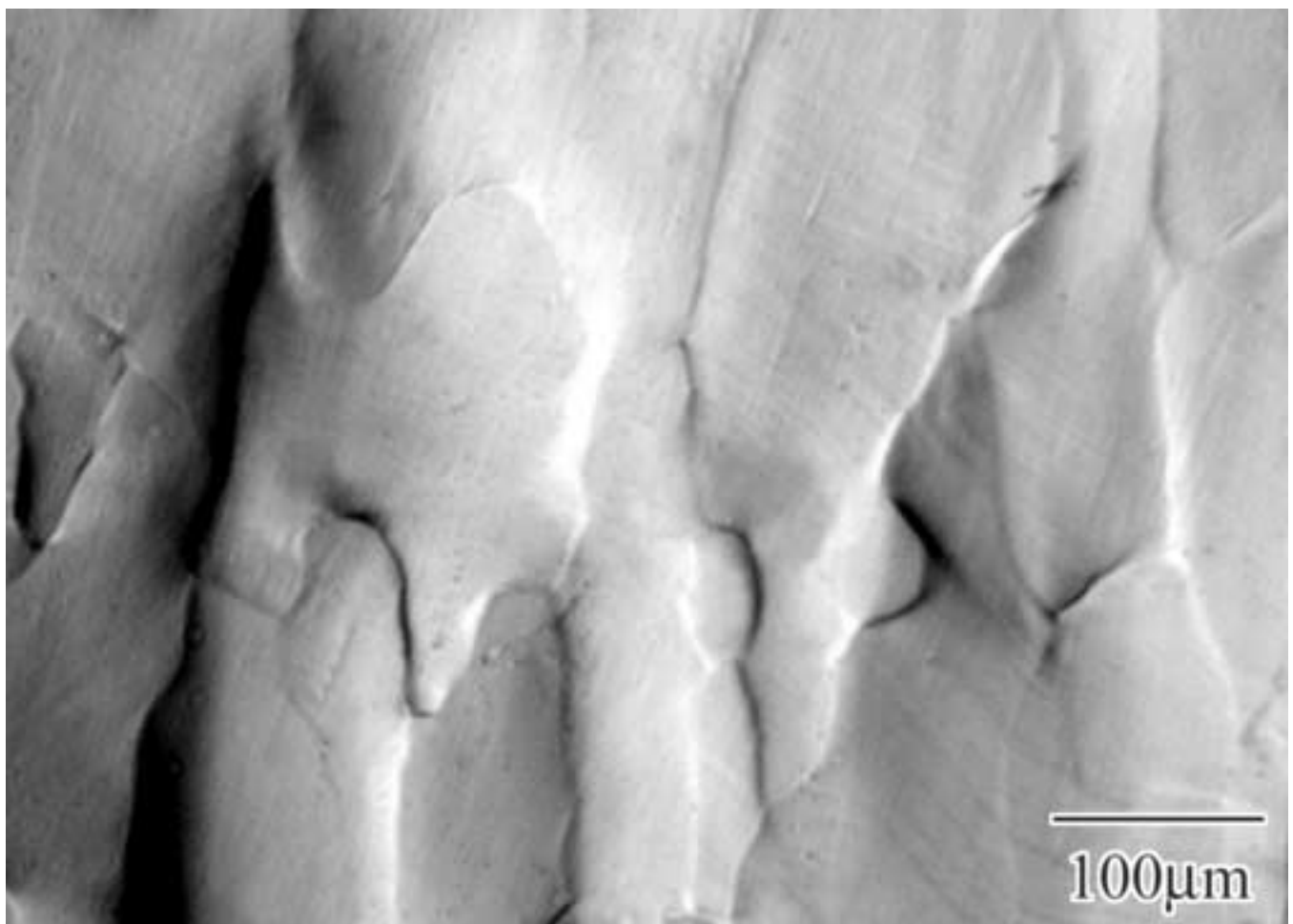
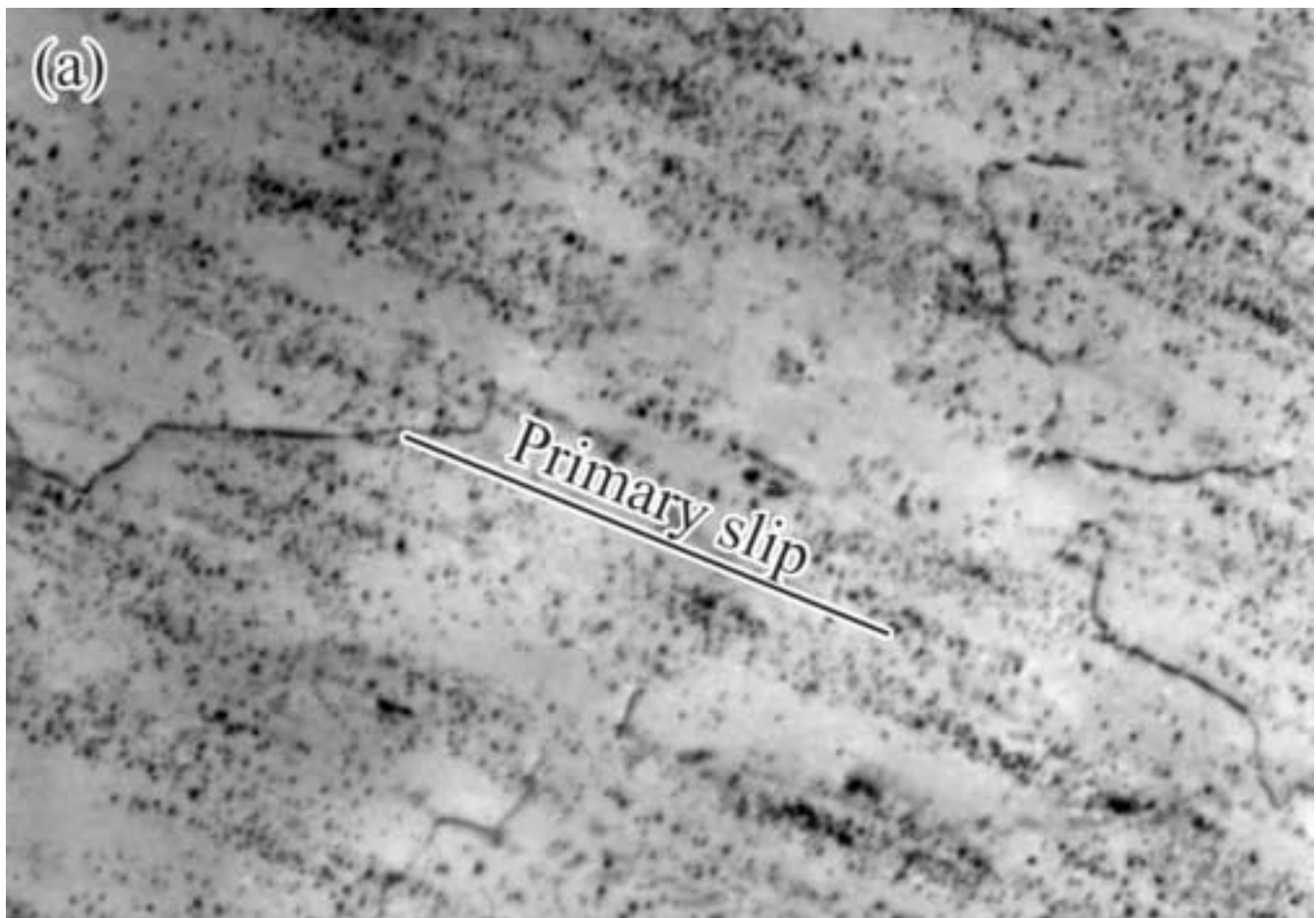


Figure06  
[Click here to download high resolution image](#)





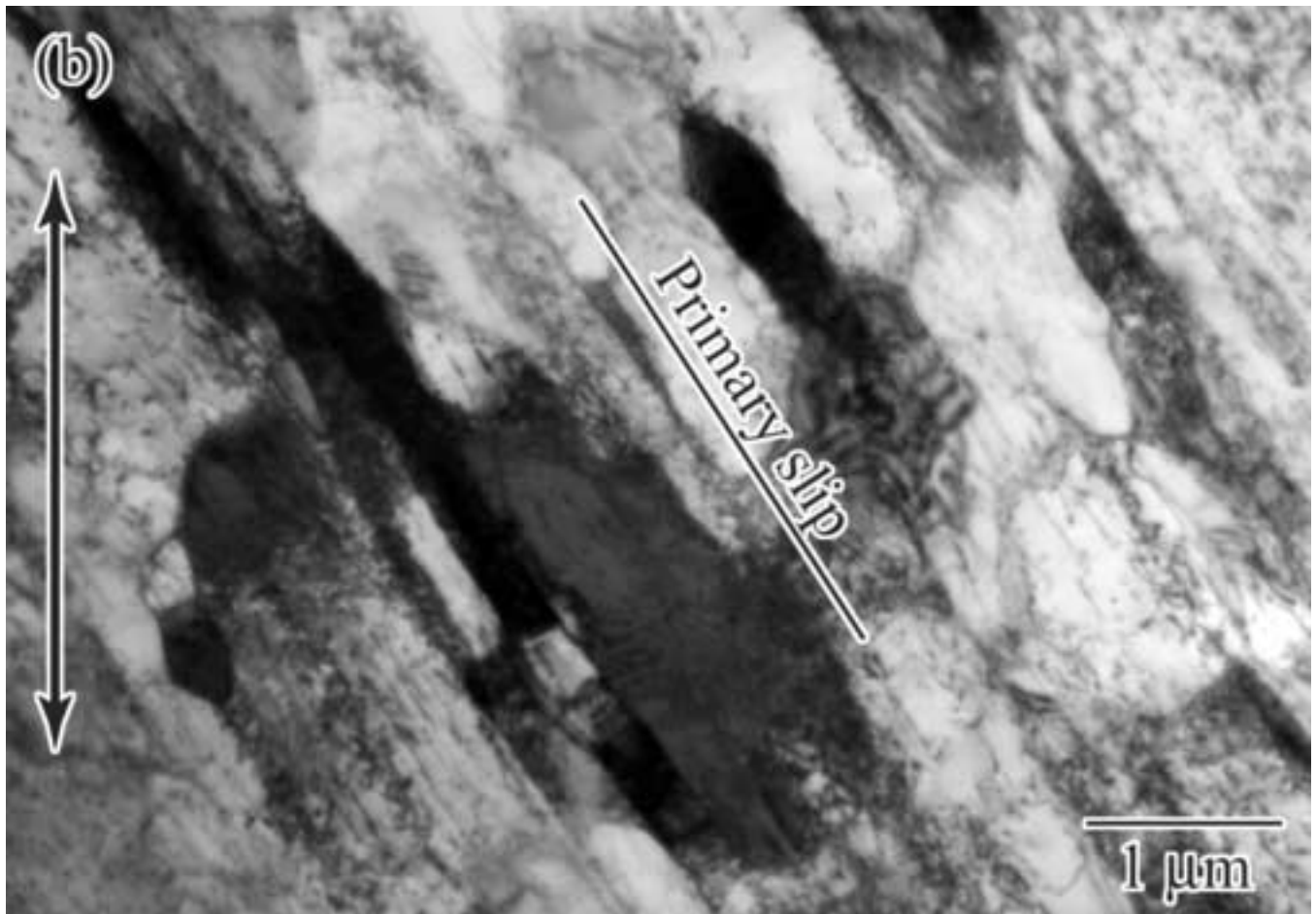


Figure08  
[Click here to download high resolution image](#)

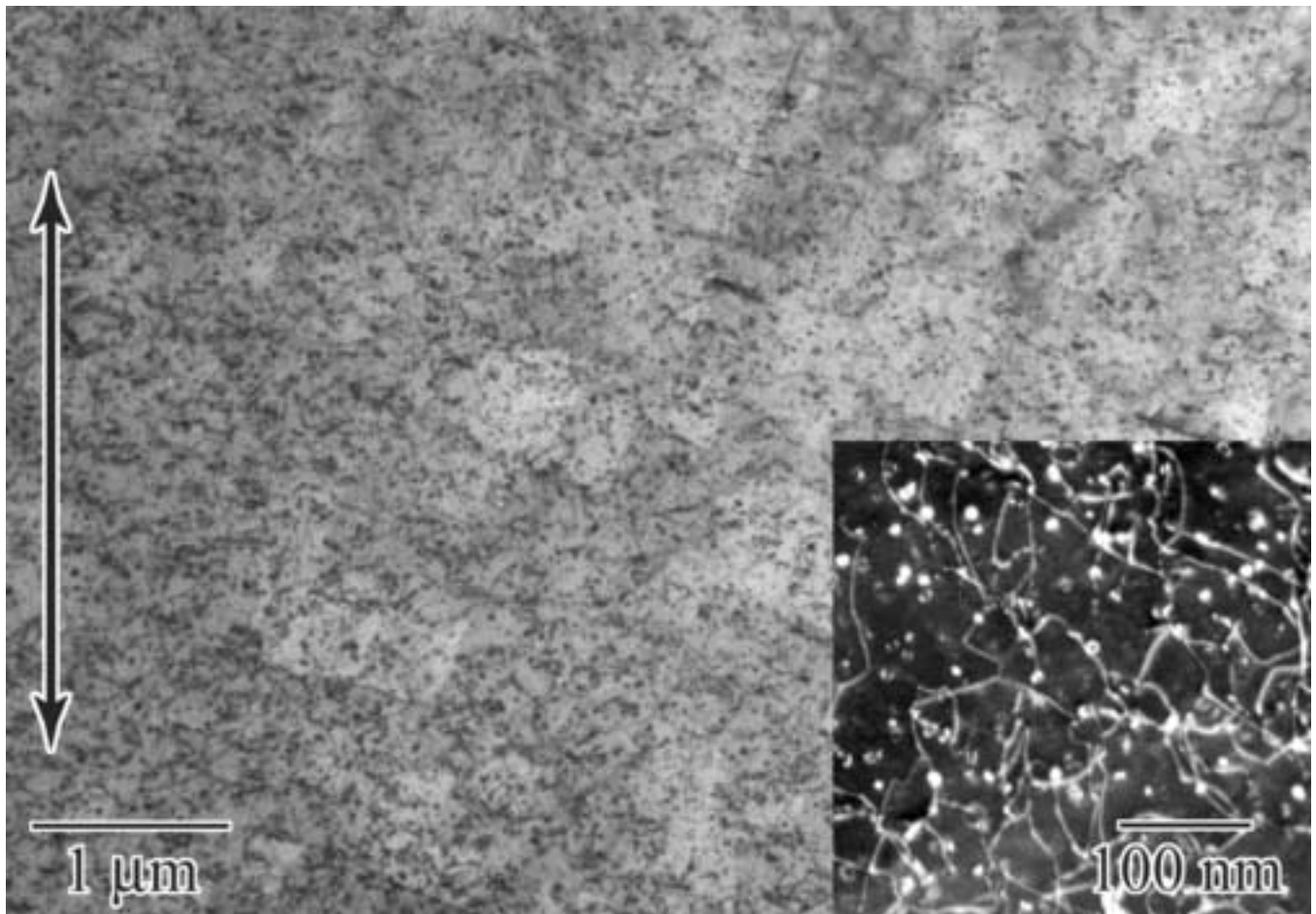


Figure09

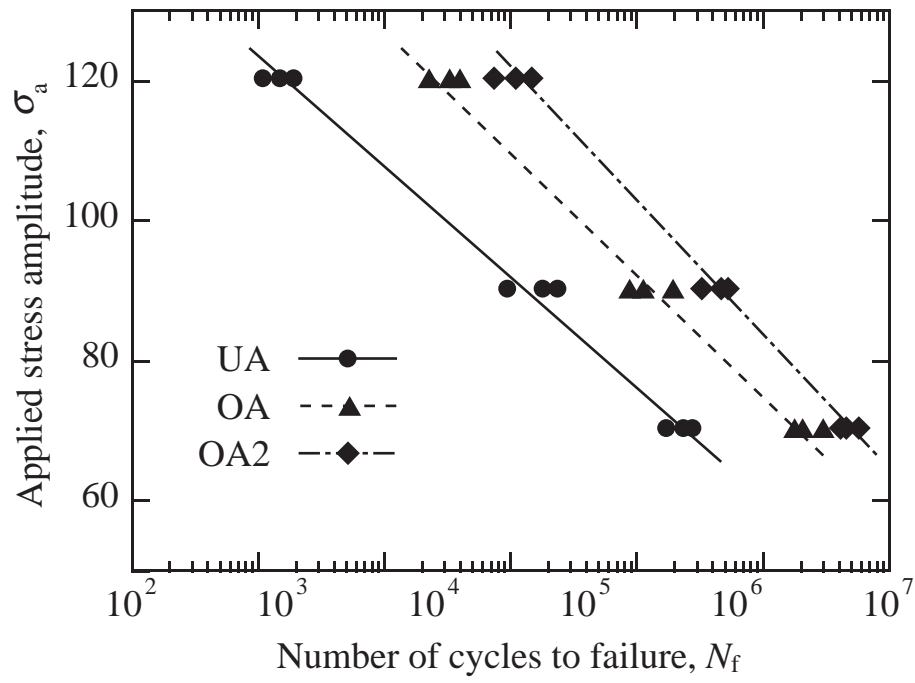


Figure10  
[Click here to download high resolution image](#)

